Superparamagnetic iron oxides nanoparticles from municipal solid waste incinerators.

Superparamagnetic iron oxides nanoparticles from municipal solid waste incinerators

FUNARI V.[1,3], MANTOVANI L.[2], VIGLIOTTI L.[3], TRIBAUDINO M.[2], DINELLI E.[1], BRAGA R.[1]

[1]*Dipartimento di Scienze Biologiche Geologiche e Ambientali (BiGeA), Università di Bologna, Bologna, Italy*
[2]*Dipartimento di Fisica e Scienze della Terra, Università degli Studi di Parma, Parma, Italy*
[3]*Instituto di Scienze Marine, Consiglio Nazionale delle Ricerche, Bologna, Italy*

Keywords: Municipal Solid Waste Incineration (MSWI), fly ash and bottom ash, iron oxides, superparamagnetic (SP) particles, anthropogenic pollution.

Highlights:

- We interrogate risky SP and iron phases pollution originating from MSWI ashes
- Magnetic techniques confirm a complex mineralogy with mixed iron oxides/sulphides
- Magnetic domain states reveal particles (often aggregate) with varying grain sizes
- Large amounts of SP grains ensue during production/management of MSWI ashes

Graphical abstract

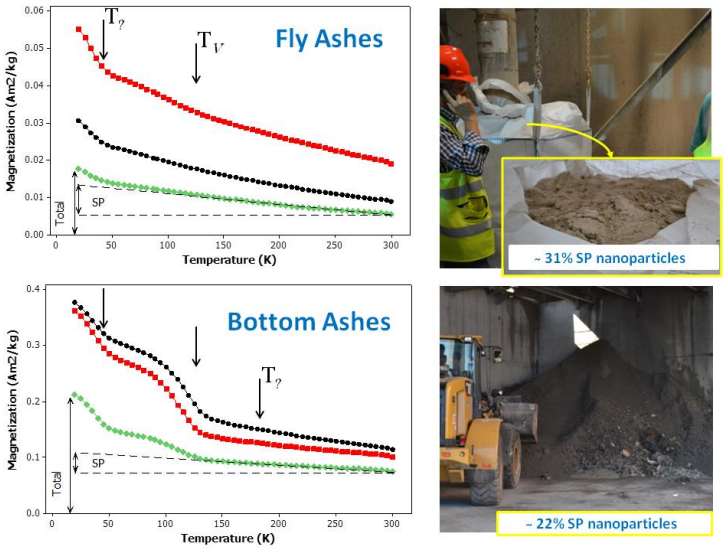

ABSTRACT

During their production, management, and landfilling, bottom (BA) and fly (FA) ashes from municipal solid waste incineration may liberate Fe-bearing, ultrafine particles and easily enter different environmental sinks of the biosphere. We aim to explore a collection of BA and FA samples from Italian incinerators to probe magnetic mineralogy and the fraction of harmful superparamagnetic (SP) nanoparticles (d<30 nm). X-ray diffraction, electron microscopy observation, temperature- and frequency-dependent magnetometry, and Mossbauer analysis are performed. The integration of information from our rock magnetic and non-magnetic techniques leads us to conclude that the dominant magnetic carrier in our samples is magnetite and its intermediate/impure forms, while sulphides (i.e., monoclinic pyrrhotite) are important ancillary magnetic phases. The SP fraction fluxing from the BA and FA outputs of a single incinerator is detected and estimated in 10^3 tons/year. This work stresses the need to calibrate the current technologies towards a safer management of combustion ashes and certainly to inform the environmental impact assessment by using a combination of different methods.

1. INTRODUCTION

Human exposure to nanoparticles pollution and environmental contamination related to Fe-bearing phases has dramatically increased during the last 30 years. It is estimated that million tons of toxic pollutants are released into the air each year [1]. Amongst these pollutants, iron- and sulphur-rich nanoparticles are liable of a range of adverse health effects in the general population, from subclinical chronic diseases to premature death [2]. Magnetite nanoparticles from particulate matter are also found in human brain suggesting a connection between the presence of these particles and neurodegenerative diseases such as Alzheimer's disease [3]. In this context, environmental magnetic studies are beneficial to explore environmental media and characterise therein contained iron minerals according to ferrimagnetic or antiferromagnetic properties [4]. Magnetic minerals can act as pollutant carriers through adsorption and structural incorporation. Some studies reported a correlation between magnetic parameters and heavy metal contents in different kinds of material, such as airborne particulate matter [5, 6], roadside pollution [7, 8], soils [9-12] lake and river sediments [13, 14], and fly ashes [15-18]. Magnetic parameters are successfully used as a tracer of a wide range of pollutants related to anthropogenic activities and also to detect particulates that strictly represent a respiratory hazard. Magnetic properties are highly sensitive to certain particle size ranges; conventional grain-size assignments (for magnetite) are: superparamagnetic (SP: d < 30 nm); stable single domain (SD: 30 nm < d < 84 nm); pseudo-single

domain (PSD: 84 *n*m < d < 17 μm); multi-domain (MD: d > 17 μm) [19]. Particles formed by combustion sources are usually fine or ultrafine [20], with a diameter in the submicron range, and have the highest potential to endanger life [20, 21]. Heavy metal concentrations in the fine particulate were found to be higher in industrial districts than in other areas [7], emphasising the health risk associated with industrial emitters and industrial processes. The particles diameter and the size distributions can vary in space and time due to differences in emission sources and atmospheric processes [22, 23]. Therefore, dust and the finest fraction of ashes generated by industrial processes gain increasing attention in environmental magnetic studies aimed to assess anthropogenic alterations of air, soil, and water. Since coal combustion represents an important world source of energy supply leading to the production of waste and dust, the iron minerals occurring in raw materials, fuels, additives, or residues are carefully studied. During such a technological process, the iron minerals are acknowledged to form highly magnetic particles with the tendency to bind hazardous elements. An extensive literature on fly ashes and polluted soils from coal-combustion power plants is available [15-18, 24]. Some works on Fe-smelters [14] and on municipal landfill leachates [25] do exist. However, the assessment of the magnetic behaviour of municipal solid waste incineration (MSWI) ashes remains largely overlooked despite their recognised hazardous nature and the nanoparticles emission is acknowledged to occur [26]. The municipal solid waste incineration (MSWI) is considered a good practice for reducing the waste volume and recovering its energy to produce electricity. Nevertheless, the risk perceived by people living near waste incinerators is very high and testified by a diffuse social response like the "*not in my backyard*". MSWI plants generate huge amounts of solid residues, around 10^4 t/a [27], and ca. 0.7 tons of gases and particulate vapour per tonne of input waste [28]. The bottom ash (BA) is the largest fraction generated in the combustion chamber; after an approximate residence time of 30 to 45 minutes on the grate furnace (up to 1150° C), the BA is usually quenched in cold water. Conversely, the particulate material from the combustion chamber is sparged to the Air Pollution Control (APC) system equipped with some flue gas treatments devices, such as scrubbers, bag filters, and electrostatic precipitators. Both MSWI ashes and MSWI emission at the stacks showed particle diameters of recognised inhalable risk [26, 29], encompassing the risk of primary and secondary pollution. The contribution of waste incinerators to the intake fraction is thought to be negligible [30], but the limited number of studies coupled with the lack of standard protocols for the risk assessment emphasises the need to further investigation.

This work aims at:

- investigating the magnetic properties of MSWI ashes from four Italian facilities;

- identifying the magnetic components liable of the strong magnetic signals observed in prior start-point measurements [27, 31];
- evaluating whether a new pollution risk related to SP grains is significant.

Spatiotemporal variations of MSWI pollution patterns are not assessed in this work. Here we provide magnetic reference data of a particular combustion product to inform pollution-related environmental magnetic studies and to assess potential health risks triggered by urban waste incineration.

2. SAMPLES AND METHODS

A collection of BA and FA samples was taken from four MSWI systems of northern Italy following the sampling methodology as in Funari et al. [32]. The selected facilities are located in four different municipalities and serve an area of about 10000 km^2 within the Po Valley. Each incinerator equipped with a grate-furnace system operates at temperatures between 850-1100° C. The solid waste input, which averages $1.5 \cdot 10^5$ tons per year, consists of 90% household waste and 10% of special waste, i.e. processing waste from steel-making industries, scraps from ceramics, automobile shredder residues, and hospital/pharmaceutical waste. The solid waste output averages $4.6 \cdot 10^4$ BA and $4.1 \cdot 10^3$ FA tons per year, respectively. The figure for BA does not include the ferrous metal scraps (ranging $5\text{-}8 \cdot 10^3$ tons per year) that are recovered by a rough magnetic separation after quenching and re-melted for reuse in an integrated system; the ferrous metal fraction is not taken in this study. The FA samples are further divided into different categories depending on the APC technology. Where it was possible, FA were collected at the first recovery phase without any treatment (untreated, FAU), after the electrostatic precipitator (FAE), and after chemical bag filters, which involved the use of soda (FAS) or lime (FAL) additives. It is recognised that samples of incinerated wastes cannot display the variability inherent in a given plant during the time and changes of the feedstock materials. Nevertheless, each sample is representative of the MSWI ash category of each MSWI plant, as determined by previous works focusing on the same materials [27, 32, 33].

We analysed BA and FA samples by a range of magnetic and mineralogical techniques. The collected materials were oven dried at 40° C for one week. The biggest metallic fragments partially melted or destroyed by the thermal treatment (d > 1 cm; mostly in BA samples) were hand-sorted and removed before the measurements. For samples with abundant magnetic materials (i.e., BA), magnetic extracts from dried and milled samples were obtained using a Nd hand magnet with a

plastic sleeve. Extracts from samples with sparse magnetic materials (i.e., FA), were collected using a Frantz magnetic separator by imparting a 1.1 A current in the laminar isodynamic region and a +15° side slope of the chute. A range of magnetic measurements was conducted on triplicate samples at the Institute of Marine Sciences of the National Research Centre (CNR-ISMAR, Bologna) and the Institute for Rock Magnetism (IRM, University of Minnesota). The chemical composition, mineralogy, and morphology were investigated by non-magnetic technique, such as XRF, SEM, XRD, at the BiGeA Department (University of Bologna) and the Department of Physics and Earth Sciences (University of Parma). Furthermore, ^{57}Fe Mössbauer spectra were measured at the IRM (University of Minnesota) on selected original samples and magnetic extracts. Further details on analytical methods are in the Supporting Information (SI).

3. RESULTS AND DISCUSSION

3.1 XRD analysis and morphological observations

The BA and FA samples show complex X-ray diffraction patterns (Fig. 1), consisting of crystalline phases and large amounts of amorphous/nanocrystalline materials. According to numerous studies, the main phases in BA consists of solid phases with high melting points already contained in the municipal solid waste feed and melt products such as glass, melitite- and spinel-group minerals [34, 35]. Conversely, FA have a quite different mineralogy ascribed to the MSWI technological process from the combustion to the subsequent flue-gas cleaning, i.e. vaporisation, melting, crystallisation, vitrification, condensation and precipitation [36]. The main crystalline phases are sulphates, carbonates, chlorides silicates, phosphates, and oxides. The phases identified by XRD analysis and their semi-quantitative estimates are reported in Table S.1. On the XRD analysis, the iron oxides result in lower amounts compared to other minerals. The XRD patterns for all our specimens show a considerable amount of amorphous or nanocrystalline materials, which is estimated around 50 wt. % BA and 15-20 wt. % FA (see SI for details).

Among the crystalline phases in BA samples, a few minerals such as quartz, gehlenite and calcium carbonates (both calcite and vaterite) are easily identified (Fig. 1a). Other mineral phases cannot be identified by a simple search-matching procedure due to a large number of overlapping peaks and to the shift of peaks position because of solid solution members. For example, the presence of plagioclase, feldspar, and pyroxene in BA is highly probable but estimating their chemical composition is unrealistic due to solid solutions and substitutions of other metal ions in the crystal lattice. Phyllosilicates (e.g., muscovite, illite), iron oxides, and a few peaks identifying

metallic aluminium are detectable as minor phases. This mineralogical assemblage is characteristic of all BA samples. The magnetic extract of BA shows the presence of iron oxides such as hematite, magnetite and wüstite. It is important to stress that the X-ray pattern diffraction of magnetite is the same of a large number of oxides with a spinel-structure like Ca/Mg-ferrite, hercynite, chromite, titanomagnetite and so on. Chemical substitutions and solid solutions in the spinel mineral are very common, signifying the possible presence of impure Fe^{2+} and Fe^{3+}oxides and iron vacancies.

Fig. 1b reports the XRD patterns of some FA categories, namely FAU, FAE, FAS and FAL collected during different steps of filtration of the APC. All the FA have a lot of chlorides and carbonates, whereas FAU, FAE and FAL also show a considerable amount of calcium sulphates, both anhydrous and hydrated. Minor amounts of quartz and calcium alumina-silicates are also detected. The FAS sample differs from FAU and FAE showing a large amount of NaCl, as a result of the soda addition, and different mineralogical phases of carbonates (i.e., trona and nahcolite) and sulphates (i.e., aphthalite). Iron oxides are present in all FA samples, but they are relatively less than those occurring in BA samples. The magnetic extract of the FAU sample doesn't help to distinguish the magnetic mineral assemblage. As for BA, the presence of titanohematite or other metals substituting in the spinel-like structures cannot be ruled out.

The SEM/EDS analysis on BA and FA (Fig. S.2) allows the observation of morphology and grain-sizes, but the identification of potential substitutes/pollutants in the different mineral phases is prevented. Both single crystals and glassy groundmass contain a significant amount of Si and Ca, but also Fe, S, Ti, and other substituting/pollutant elements (e.g., Zn, Pb, etc.). Iron results in association with Ca, Si, S, Ti, and other heavy metals. Some particles can be very small, with diameters well below the micron range, overcoming the instrument resolution. Therefore: i) pollutants may enter both crystalline and glassy phases, including those capable of a certain magnetic response; ii) magnetic carriers are most probably minor phases, in form of impure oxides, sulphates/sulphides (e.g., $Fe_2(SO_4)_3$, pyrrhotite, greigite), carbonates (e.g., siderite), alloys; iii) the amorphous phase might be responsible for unaccounted magnetisation.

a)

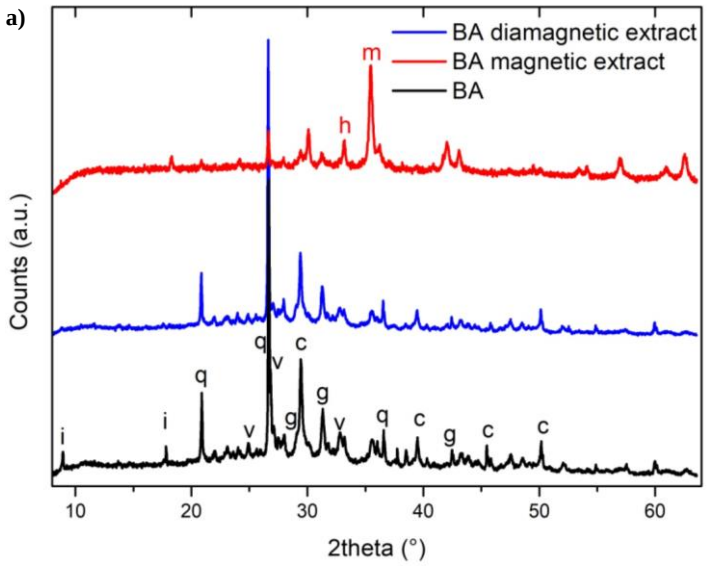

b)

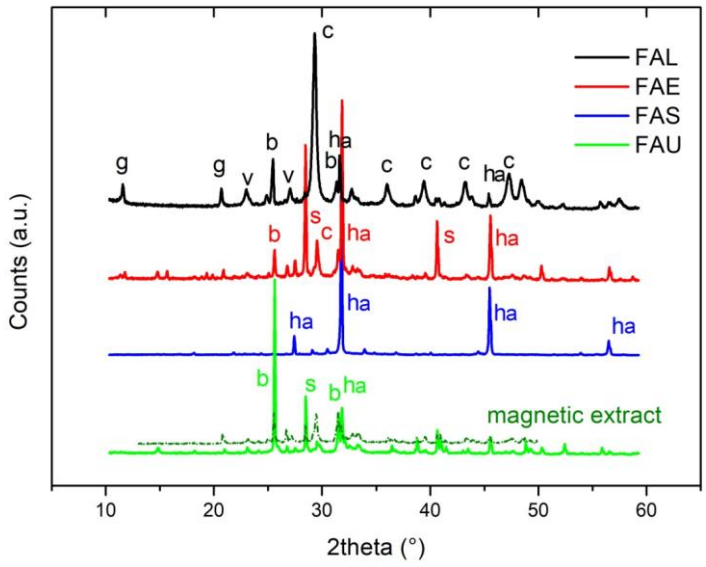

Fig. 1 XRD spectra of representative samples of **a)** BA and **b)** different FA types, including magnetic extracts. For **a)**: *i* = illite, *q* = quartz, *v* = vaterite, *g* = gehlenite, *c* = calcite, *m* = magnetite, *h* = hematite; for **b)**: *g* = gypsum, *v* = vaterite, *b* = bassanite *c* = calcite, *ha* = halite, *s* = sylvite; FAL = bag filter fly ashes treated with lime; FAE = fly ashes from electrostatic precipitator; FAS = bag filter fly ashes treated with soda; FAU = untreated fly ashes.

3.2 Mössbauer spectroscopy

Mössbauer spectra (Fig. 2) and fitted parameters (Table S.2) for two selected samples of BA and FA are reported. The Mössbauer spectrum of the FA sample has not displayed any signal, but we were able to process the signal of a magnetic extract of the FA material. The obtained spectra of BA and FA samples show considerable differences. In the BA sample (Fig. 2a), the sextets indicate the two molecular geometries of magnetite (representing 34% of the whole spectrum) with their characteristic parameters. However, the hyperfine field of Bhf for the sextets shows anomalies that might relate to the presence of metallic iron, alloys, or magnetic sulphur minerals. The two central doublets (i.e., 3 and 4 in Table S.2) with isomer shift close to 1 mm/s are characteristic of Fe^{2+} [37]. The high quadrupole splitting of doublets 3 and 4 might indicate either Al/Ti substitution in spinel-like structures (i.e., $FeAl_2O_4$, $TiFe_2O_4$) or Fe^{2+} sulphides. The doublet 5 with a small isomer shift may correspond to SP hematite, but the high quadrupole splitting might indicate Fe^{3+} ions in carbonates/sulphates/silicates structures [5] as a superimposed signal. The FA sample (Fig. 2b) is composed of two sextets with the characteristic Mössbauer parameters corresponding to magnetite. The magnetite phase looks ferric (maghemitization) due to the low IS and cation substitution may account for the observed low Bhf. The doublet 3 corresponds to a Fe^{3+} phase, but its large line width (0.85 mm/s) most likely points to a superposition of, at least, two Fe^{3+} doublets which cannot be resolved. Noteworthy, the FA sample produced the so-called "intermediate relaxation" effect due to SP grains, which translates in a collapse of the sextet in favour of a paramagnetic doublet or singlet. The signal from this phenomenon was removed prior to fitting, so any contribution from that material is not in the fitted spectra and might have reduced the number of recognised doublets. To a lesser extent, the BA sample displayed an intermediate relaxation effect that, however, was not so high to force changes in the standard fitting procedure. The cations distribution deduced from these measurements is the following: Fe^{3+} and Fe^{2+} ions account for ~32% and ~68%, respectively, of the total iron atoms in the BA sample; for the FAU sample, almost all the iron atoms are Fe^{3+} and only 7% Fe^{2+} ions. These estimates assume that magnetite is stoichiometric (i.e., that 2/3 of the total Fe in magnetite is Fe^{3+} and 1/3 is Fe^{2+}) and thus possible errors may derive from the assumption of perfect stoichiometry.

Observed spectra and iron states in our samples markedly differ from data of coal fly ashes [38, 39] and other anthropogenic dust from industrial emitters [18] as well as from urban atmospheric particulate matter [5]. Conversely, the obtained spectra are similar to those reported earlier by Fermo et al. [40] for a FAE sample collected from a MSWI plant that probably adopted a

similar incineration technology. Fermo and co-workers recognised hematite, but they had difficulties in identifying other lines probably due to SP-related effects.

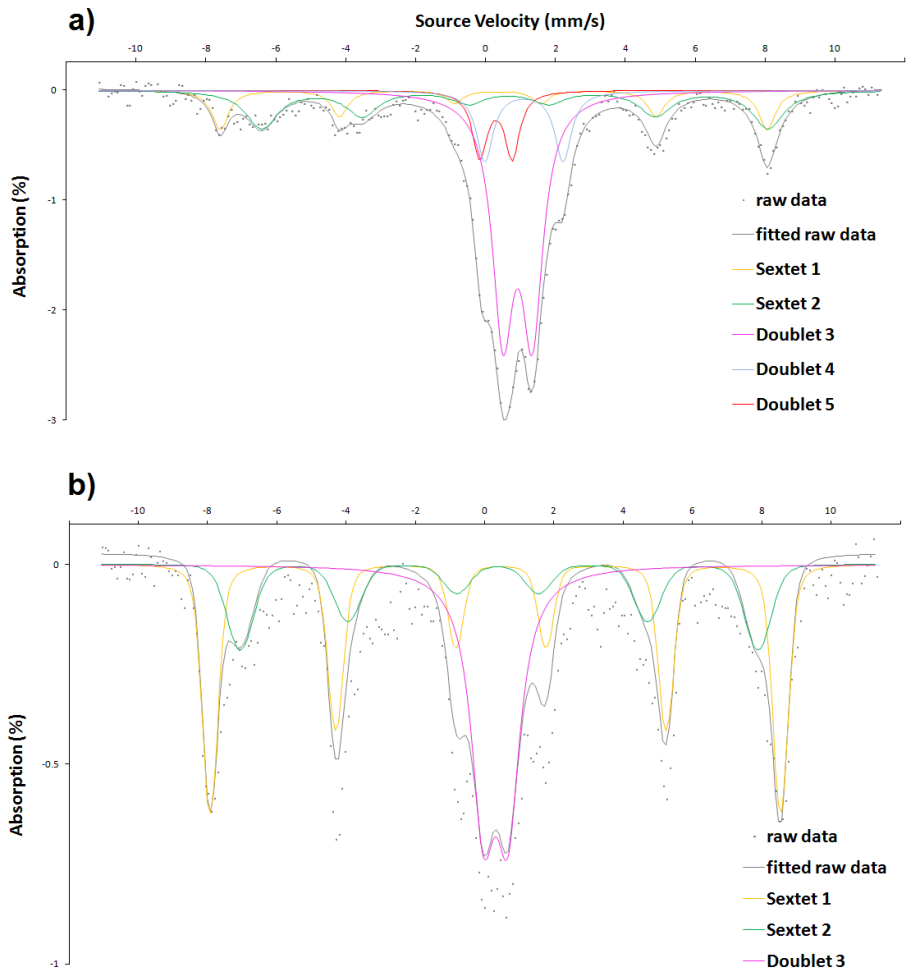

Fig. 2 Mössbauer spectra of representative BA (a) and FA (b) samples, recorded at ~85 K. Deconvolution fits using Lorentzian line shapes algorithm are provided. Fitting reliability can be assessed by comparing the raw data points (dots). The spectrum in b results from a FAU magnetic extract since original material produced a very weak signal. Further details on experimental conditions are provided in SI.

3.3 Thermomagnetic analysis

The analysis of the thermomagnetic curves of BA and FA samples indicates that magnetite with its characteristic Curie temperature (T_C) of ~580° C is the main ferrimagnetic phase (Fig. 3). The T_C of the FA sample (Fig. 3b) is slightly below 580° C likely due to a higher presence of impure magnetite than in BA. The first derivative of the heating-cooling lines for the BA sample also shows peaks at ~300° C, unlike FA, that might represent the contribution of other carriers of magnetic signal such as sulphides or native metals (e.g., Ni). In many cases, the first derivative of the thermomagnetic curves for FA samples reveals a slight decrease of the heating curve near temperatures between 500-550° C, which can be related to magnetite with a variable composition (cation substitution). These peaks might reflect the presence of Ca/Mg-ferrite [18] that is likely sourced from the lime/dolomite addition. Heating and cooling curves show that no significant mineralogical changes occur during heating, while a certain proportion of weak magnetic minerals may turn into stronger ones at high temperature, so susceptibility is higher during cooling. Evidence of maghemitization is also found in BA samples in the first part (up to 500° C) of the thermomagnetic lines where a susceptibility gain occurs (Fig. 3a). The hypothesis of a contribution of maghemite transforming to hematite cannot be rejected especially in the BA sample, where the susceptibility is not zero after 580° C. However, the diagnostic feature of maghemite (which T_C is ca. 650° C) is not observed. During cooling of both samples, the magnetisation is almost completely reversible until the T_C and then shows an increase in κ at the end of the run. Unlike the BA thermomagnetic curves that display the characteristic shape of ferrimagnetic components, the heating-cooling curves of all the FA samples reach the maximum of κ at room temperature. This feature points to a contribution of paramagnetic phases that adds to the ferrimagnetic components.

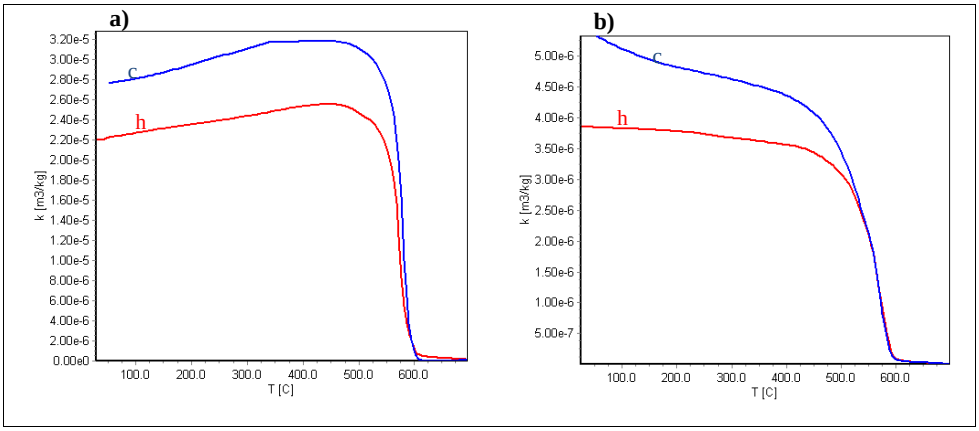

Fig. 3 Thermomagnetic curves of selected BA (a) and FA (b) samples in an air atmosphere. κ = magnetic susceptibility, T = temperature, h = heating line, c = cooling line.

3.4 Hysteresis properties

The MSWI samples are characterised by narrow hysteresis curves (SI) that saturate below ~200 mT and low coercivity (B_C range: 7.2 – 14.1 mT), indicating the predominant contribution of low coercivity ferromagnetic minerals such as magnetite. Both MSWI samples produce tall, thin hysteresis loops typical of pure magnetite with a significant reversible component of the magnetisation [4]. The uncorrected loops (Fig. S.3) indicate a higher contribution of paramagnetic/diamagnetic components in FA than in BA. Moreover, the hysteresis curves resemble the typical loop of SP grains, showing a steep magnetisation versus field curve which saturates at low fields [19]. Variations in grain-size play a major role in determining the shape of the curve [4]; we hypothesise that the shape of the overall loops is the combination of MD and SP magnetite grains, with a larger contribution of pure MD magnetite in BA sample than in other FA [19]. The BA samples show a slightly larger B_C than FA samples, averaging 10.5 mT and 8.6 mT, respectively. The relatively high values of coercivity of remanence (B_{0CR}), ranging 24 – 52 mT, confirm the presence of strong ferro(i)magnetic components. These differences in the mean values of B_C and B_{0CR} also confirm that the magnetic grain-sizes in FA are finer than those in BA. Hematite, which usually results in flat, fat loops, often not saturated, seems absent or, at least, occurs at low concentrations that do not affect the shape of hysteresis curves. The fact that hematite is 200 times less susceptible to magnetisation further supports this observation.

3.4.1 Analysis of FORC distribution

First order reversal curve (FORC) diagrams provide further information from hysteresis loops that is unavailable from standard measurements. A FORC diagram is calculated from a suite of partial hysteresis curves, which are measured by saturating a sample with a large positive field followed by a step-wise decreasing reversal field [41]. FORC diagrams for both BA and FA samples (Fig. 4) show a strong coercivity peak around 10 mT and a strong interaction fields (Hu) spreading asymmetrically to high coercivities (± 80 mT BA; ±40 mT FA), signifying a prevalent ferro(i)magnetic component. A broad, not well-defined, central ridge with a long tail along the Hc axis up to 100-150 mT characterises BA and FA samples and is indicative of the coexistence of hard magnetic phases. Former studies indicated that traffic related ferrimagnetic grains consist of partially oxidized magnetite particles, in the form of a magnetite-like core covered by an oxidized cation-deficient maghemite-like coating (Muxworthy et al., 2003; Sagnotti et al., 2009). This oxidized coating may be responsible of the coercivity tail extending beyond the typical range for

stoichiometric magnetite. Asymmetry and negative regions are commonly seen in FORC diagrams of MSWI ashes. The origin of asymmetry and negative regions is ascribable to an artefact of the fitting procedure, the presence of hard magnetic phases (hematite, sulphates/sulphides, and carbonates), or magnetostatic interactions. This observation suggests that a hard phase is well mixed with a softer phase like magnetite: the overall FORC distributions are likely a result of homogeneous mixtures of different mineralogical phases, which overlap and combine to give a single distribution [42]. All the FORC distributions are representative of a PSD magnetic assemblage, therefore with transitional behaviour between true MD and SD grains. The presence of closed contours near the maximum distribution peaks further points to fine SD and PSD grains as the prevalent magnetic fraction. The FORC diagram representative for BA materials (Fig. 4a) is typical of PSD materials and approaches the reference diagrams for synthetic aluminous iron oxides and those for natural sulphidic sediments [43]. The FA materials express a similar FORC distribution which is, however, transitional towards SP materials (compare FORC distribution for SP greigite [43]).

Commentato [VF1]: Suggerimento di un revisore ma non aggiunge molto a mio avviso…. Non so se metterlo

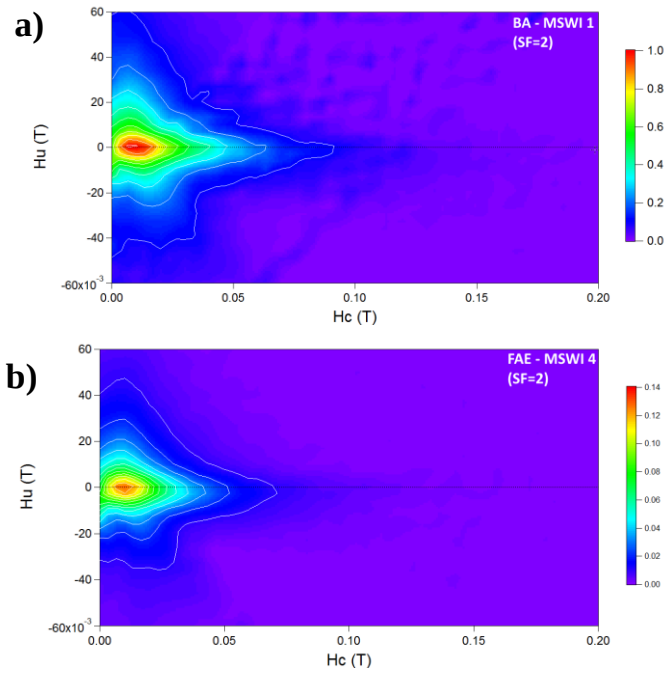

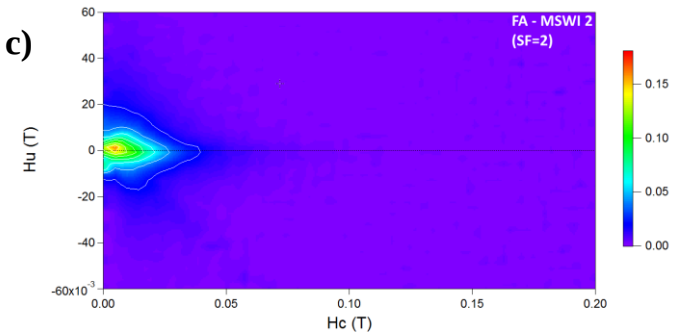

Fig. 4 - First-order reversal curve (FORC) diagrams for representative samples of BA (a), FAE (b), and FAU (c). The FORC diagrams are computed using FORCinel software [44] that allowed the processing with optimum smoothing factor (SF), magnetic drift and first point artefact corrections.

3.5 Magnetic susceptibility of MSWI ashes

Fig. 5 plots the mass specific magnetic susceptibility (χ) and its frequency dependence (κ_{fd}) (see SI). The susceptibilities clearly cluster BA and FA samples. The magnetic extracts (closed symbols in Fig. 5) are also separated accordingly, even though the magnetic separation is less efficient for FA than BA as suggested by the spread in the χ ranges. The average χ values of BA samples range 179-226 $\times$ 10^{-8} m^3/kg, being the highest χ value 362 $\times$ 10^{-8} m^3/kg. The FA samples show χ values about one order of magnitude lower than those for BA, averaging 20.2 $\times$ 10^{-8} m^3/kg. These data are in agreement with previous magnetic measurements on MSWI ashes [27] and partly lie within the range of χ values for MSW landfill leachates (64-970 $\times$ 10^{-8} m^3/kg) [25] and other incineration residues such as coal fly ashes (306-4804 $\times$ 10^{-8} m^3/kg) [17, 18]. The χ measurements of MSWI ashes reported here are consistent with those of sediments near Fe-smelters (200-600 $\times$ 10^{-8} m^3/kg) [14] as well as they closely agree with the χ values of residues after lignite burning, cement dust, and coke dust (579, 146, 356 $\times$ 10^{-8} m^3/kg on average, respectively) [18]. The FA samples from bag filters, especially FAS, experience low susceptibilities (2.3-14 $\times$ 10^{-8} m^3/kg) as a likely consequence of low iron contents in those materials. The intensities of the measured susceptibility are proportional to the average iron contents determined by XRF (Table S.4), indicating Fe-bearing minerals are chief carriers of the magnetic signal. Also, the lower susceptibilities are ascribable to a higher proportion of total iron contained in paramagnetic minerals (this mainly pertains the FA samples).

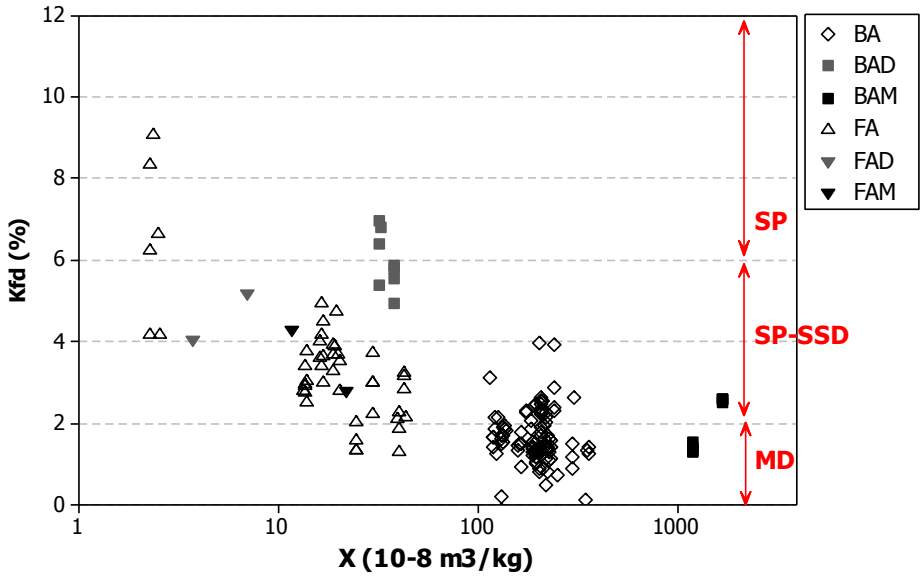

305

306 **Fig. 5** Frequency dependent susceptibility (κ_{fd}%) vs. mass specific magnetic susceptibility (χ) for BA and FA
307 samples, including their magnetic extracts (where the suffix M= magnetic; D= (more) diamagnetic).
308 Magnetic state domains boundaries as defined by Dearing et al. [9].

309 A characteristic feature of MSWI ashes is the relatively high percentages of κ_{fd}, exceeding the
310 2% in most of the measures and reaching peaks greater than 8% for a few samples, in agreement
311 with the first measures of magnetic susceptibility on MSWI ashes [27]. The BA samples (1.7 κ_{fd}%
312 on average) show lower κ_{fd} values with respect to the FA ones (3.6 κ_{fd}% on average) whence
313 maxima are recorded for the samples that belong to the FAS category. Values of κ_{fd}% similar to
314 those observed for MSWI samples are quite uncommon amongst anthropogenic materials. For
315 example, magnetic measurements on solid industrial end-products from thermoelectric power plants
316 and steelworks resulted in κ_{fd}% averages narrowly at, or below, the 2% threshold [16]. Coal fly
317 ashes despite high χ averages, experience lower κ_{fd}% values compared to those from MSWI FA
318 [45]. Nonetheless, a wide range of materials of both geogenic and anthropogenic origin such as
319 Chinese loess, pedogenetic soil horizons, urban topsoils, street dust, and urban particulate matter,
320 have levels of κ_{fd} comparable to MSWI samples [7, 12, 46]. Many authors reported that these
321 materials characterised by a high κ_{fd} parameter have abundant SP-sized grains. Fig. 5 shows that
322 more than 50% BA samples are MD-dominated, while the remaining BA lie within the SP-SSD
323 region. It is worth noting that the BA (more) diamagnetic extracts experience higher κ_{fd}% than the

magnetic ones, indicating a potential contribution of SP grains in the BA materials. Conversely, the most of FA is in the SP-SSD region, and some are in a SP state. According to the semi-quantitative model by Dearing et al. [9], MSWI samples result in relatively high contents (>10% on mass weight) of SP particles overreaching the 2% κ_{fd} threshold in the majority of samples. Anthropogenic magnetic minerals are usually large magnetic grains in a MD state, but the χ_{fd} parameter for MSWI ashes likely indicates admixtures of SP and coarser non-SP grains, being the latter component MD/PSD-dominated.

A contribution of the SP fraction derived from the κ_{fd} parameter can be misinterpreted for rather varying mineralogical assemblages and needs to be further supported by more robust means, for example by temperature-dependent data. We attempt to quantify the SP fraction of MSWI ashes in a section sotto, where a comparison with other techniques such as low-temperature remanence/susceptibility measurements [47, 48] is provided.

3.6 Magnetic Properties Measurement System (MPMS)

Selected BA and FA samples were measured using the MPMS to probe in detail magnetic mineralogy and eventual SP behaviour. In Fig. 6, low-temperature remanence curves are obtained by first imparting a 2.5 T SIRM at room temperature (RTSIRM) and measuring during zero-field cooling (ZFC) to 20 K (RT remanence on cooling), and then imparting a 2.5 T SIRM at low temperature (LTSIRM) and measuring while zero-field heating back to room temperature from 20 K (ZFC, remanence). Further details regarding the acquisition procedure are provided elsewhere [49]. The measured sequences show magnetite-like shapes for most of MSWI samples. Nonetheless, the low-temperature remanence curves of BA and FA samples have distinct shapes in agreement with the preliminary observation reported in [31]. The BA samples systematically show a dramatic loss of remanence between 100 K and 130 K during zero-field cooling (Fig. 6a). This drop, associated with the isotropic point and the Verwey transition, confirms that magnetite is the main remanence carrier in BA material. This feature is recognisable for the reference curves of coarse-grained magnetite albeit the drop of remanence in pure MD magnetite is very sharp and narrower at 120 K. Most probably, the observed curves for BA samples are characteristic of mixtures of coarse (e.g., MD) and fine (e.g., SD/PSD/SP) grains and adhere, for example, to reference curves of pozzolanic materials [50]. BA curves display an additional small drop on cooling at about 190 K (Fig. S.4) that may be due to nanohematite [51]. Conversely, the ZFC LTSIRM warming curves of FA samples show a steep decrease at very low temperatures and monotonically decrease after ~40 K. The room-temperature remanence shows a flat trend, which is expressed by 90% of the FA samples in this study (the remaining 10% shows almost the same

behaviour of BA samples). The Verwey transition in FA samples is not clear probably due to the presence of oxidised/impure magnetite or unblocking of SP grains. Overall, the behaviour of the remanence for FA samples suggests the presence of finer grains than those occurring in BA materials as well as a crowd of minerals much more oxidised (or hydrated). The measured curves of FA samples resemble those of maghemite or pozzolanic ash.

The Verwey transition typically occurs at ~120 K in stoichiometric magnetite, but the observed Verwey transitions for MSWI ashes occur over a broad temperature range (i.e., 110-130 K), indicating nonstoichiometry (see also Fig. 6) and the presence of grains partly oxidised (i.e., maghemitization). According to the first derivatives of the ZFC-FT curves (Fig. S.4) and the remanence changes associated with the Verwey transitions, it is clear that magnetite is less oxidised in BA than FA. Other phase transitions occur in BA and FA samples over characteristic temperature ranges, which are liable of the remanence carried by different minerals. Phase transitions of FA samples are less clear than those of BA samples, but still present (Fig. 6a and c). A phase transition at about 30 K on ZFC curves is always present and visible both in BA and FA samples. This might indicate either i) the presence of siderite ($FeCO_3$) that experiences a magnetic transition at ~38 K or ii) the Besnus transition (30-34 K) diagnostic of monoclinic pyrrhotite, despite it is not visible in the RTSIRM cooling curves, or iii) most likely, an effect due to a poorly-understood electronic relaxation phenomenon in pure and oxidised magnetite at that T. The RT curves of both BA and FA sample reveal weak magnetic transitions at ~260 K and ~190 K (see also Fig. S.4) probably corresponding to the Morin transition for α-Fe_2O_3 hematite and nanohematite, respectively. Measurements of AC susceptibility by MPMS (Fig. 6b and d) support a significant contribution of SP grains especially in FA materials. FA samples show larger frequency dependence than BA and the temperature of the peak in both in-phase and out-of-phase susceptibility (X′ and X″ in Fig. 6), which corresponds to the blocking temperature, is shifted towards lower temperature (~30 K for FA; ~50 K for BA). Both in-phase (X′) and out-of-phase (X") susceptibilities are one order of magnitude higher in BA than in FA. The increased amplitudes in BA samples can be due to either one or a combination of the following factors: i) conductive eddy currents, indicating the presence of native metals or graphite; ii) high contents of pyrrhotite, hematite, iron or titanomagnetite; iii) significant SP/SD presence [19]. The MPMS measurements confirm the presence of a significant population of SP grains in FA samples, and a less significant but still detectable SP population in BA samples. In general, mixed mineral assemblages encompassing impure (titano)magnetite, (titano)hematite, ilmenite, pyrrhotite, and native metals are characteristic of these anthropogenic materials and may conceal the real SP contribution.

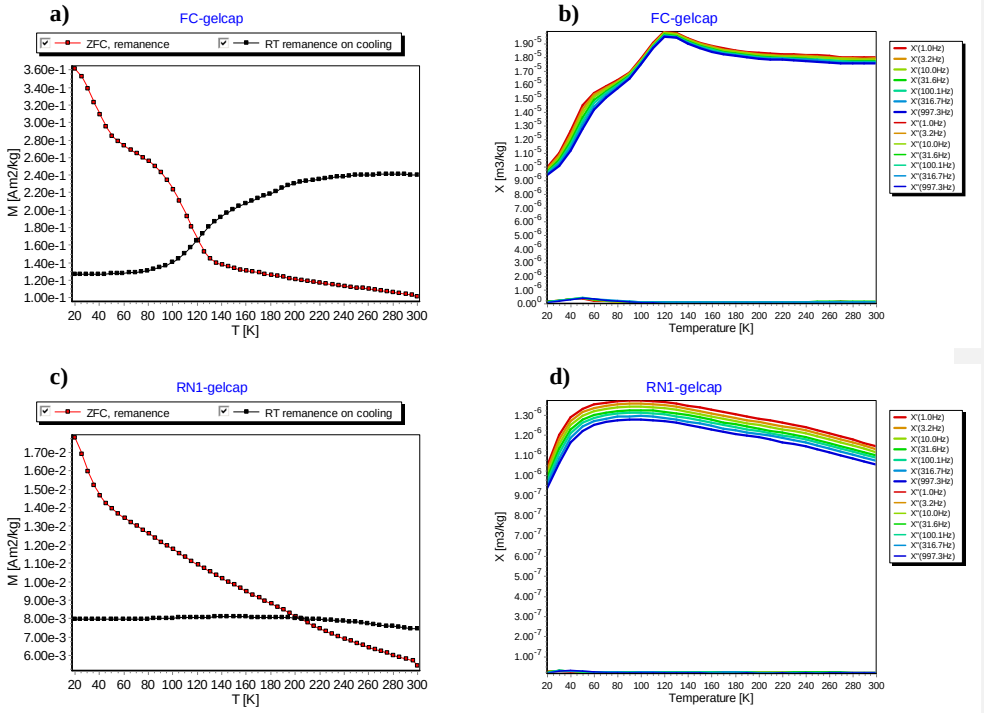

Fig. 6 MPMS measurements of representative BA sample (above) and FA sample (below). Low-temperature remanence curves (a, c) during zero-field cooling to 20 K (RT remanence on cooling) and on heating back to room temperature (ZFC, remanence). AC susceptibility (b, d) is measured at 7 different frequencies and in fixed field amplitude as a function of temperature; both in-phase (X') and out-of-phase (X'') susceptibility are displayed.

3.6.1 Estimation of the SP fraction

The low-temperature remanence curves in Fig. 6 display a steep decay between 20 and 40 K for both samples and another steep drop between 100 and 120 K for the BA sample, superimposed on a smooth monotonic decrease towards ambient temperatures, which may be attributed to the progressive unblocking of the SP population. Other evidence of a SP contribution in both BA and FA obtained from previous sections (e.g., the χ_{fd} parameter, the hysteresis properties) adds to this observation. Although a magnetic method that provides a quantitative measure of the amount of SP grains in environmental or anthropogenic sample materials doesn't exist, Banerjee *et al.* (1993) proposed a method based on thermal unblocking of LTSIRM for a quantitative estimate of the SP fraction (d < 30 nm) of magnetite. By using the same approach, we tried to measure the real contribution of SP grains on the magnetic response. The Fig. 7 attempts to compare low-temperature thermal demagnetization of the SIRM for several BA and FA samples and to apply the

Eliminato: Fig. 7

graphical interpretation technique. The general loss of remanence between 20 K and 300 K indicates a significant presence of SP nanoparticles; while the slightly different slope amongst the samples in Fig. 7 suggests a small variation in grain-size distribution of magnetic particles. The contribution to the remanence of SP grains can be determined by subtracting both the value of the thermally-stable 300 K remanence (from the whole curve) and the remanence lost during the T_V (the specific temperature value of T_V was extrapolated from the first derivative of the remanence curve for each sample). The values for SP content obtained using the graphical method point to a SP fraction in the range of 16-22% in BA samples and a 25-31% SP fraction is found in FA samples. Although Fig. 7a and b show the simultaneous presence of large and small grains in both BA and FA samples, the contribution of SP grains is considerable and relatively higher in FA rather than BA as argued before. Very interesting observations are the following: i) since the BA samples have a lower SP fraction compared to FA samples, most of the SP grains are probably carried from the combustion chamber to the APC system; ii) the largest content of SP grains is estimated in FAU, which represents the material recovered from the first section of filtration [33], suggesting that most of the SP grains are not caught by the subsequent steps and are thus released in the atmosphere. In addition, the values for SP content obtained exploiting the ratio χ to SIRM [48] compare favourably with the more reliable thermal demagnetization of low-temperature SIRM technique: SP fractions lie in the range 10-35% and 26-58% for BA and FA, respectively. In this case, the increases of χ/SIRM (assumed to be due to SP grains) are measured with reference to a baseline, which was selected to be the lowest measured χ/SIRM value. These estimates are conservative because we measured, with all probabilities, only a fraction of SP grains that survives to preserve this signal. Moreover, diverse oxidation levels in BA and FA magnetic minerals translates in an artificial lowering of SP/total ratio [52] and the probable presence of iron oxyhydroxides (e.g., the RT-ZFC curves likely contain a signal from ferrihydrite) could result in a further underestimate of the SP fraction using the low-temperature technique [48].

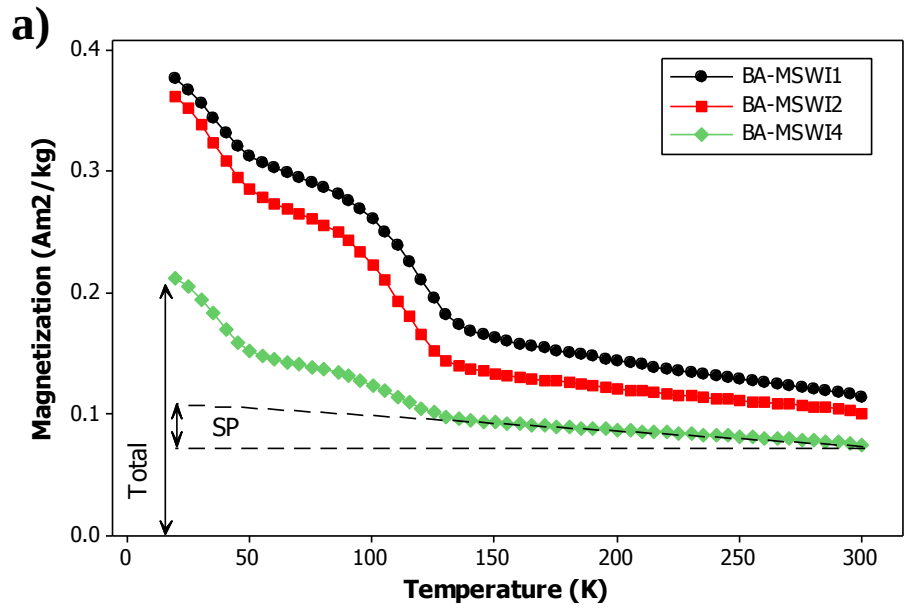

433

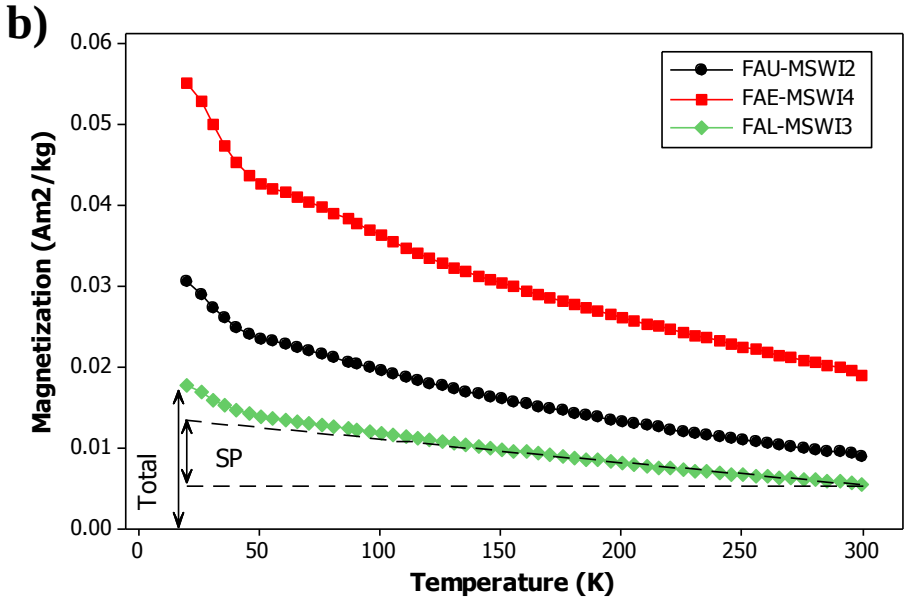

434

435 **Fig. 7** Low-temperature thermal demagnetisation of a SIRM imparted at 20 K, for representative samples of
436 BA (a) and FA (b). Ashes deriving from different MSWI plant and different FA categories are also
437 indicated. Note the graphical analysis according to the method of Banerjee et al. (1993).

4. CONCLUDING REMARKS

4.1 Disentangling mixed magnetic mineral assemblages of Fe-bearing phases

The high values of magnetic susceptibility (χ) of MSWI ashes (Fig. 5) and their direct relation to the total iron contents (Table S.4) suggest that iron oxides are the dominant magnetic carriers, irrespective of the MSWI combustor designs and heterogeneous waste feed. All the magnetic measurements verified the chief role of magnetite-like phases in both BA and FA samples. According to the Mössbauer analysis, the magnetite to hematite ratio is higher in BA than in FA samples. The low content of magnetite in FA results in lower χ values compared to those of BA. A large amount of hematite in FA reasonably depends on the lower temperature profile and the different oxygen pressure within the APC system. A contribution of hard magnetic phases and paramagnetic minerals has been proven for both BA and FA samples, but the ferro(i)magnetic component of BA is found to be overwhelming. The strong magnetic signal of BA samples likely depends on iron oxides sourced from waste metal fragments that were assimilated by melting and later re-crystallized during incineration and quenching. Conversely, the chemical additives used in the APC system virtually dilute the ferro(i)magnetic component of FA. The magnetic spinels found in MSWI ashes, especially those occurring in FA, are ferrite according to the temperature-dependent data. Ferrimagnetic intermediate titanohematite and titanomagnetite can occur in FA and BA, respectively (FeO-TiO_2-Fe_2O_3 ternary diagram in Fig. S.5), and add to the overall magnetic response.

Nonstoichiometry is pervasive for minerals in MSWI ashes as suggested by the MPMS transition temperatures. The simultaneous presence of magnetite, maghemite, and hematite confirmed by rock magnetic measurements and wüstite inferred by the XRD analysis, emphasises complex pathways of mineral formation. Intermediate phases with iron vacancies and substitution of di- and tri-valent metals occur in BA and FA sample from MSWI, as argued for other anthropogenic materials [15, 45]. Many magnetic measurements may infer hard magnetic phases such as greigite, monoclinic pyrrhotite, antiferromagnetic oxides, and siderite, but they are hardly confirmed. The Mossbauer analysis apparently detects magnetite and hematite alone, but the following factors may have concealed other Fe-bearing minerals: the thermal relaxation effect, overlaps of (sub)doublets, anomalies of the hyperfine field of Bhf, and a considerable amorphous phase. The coarse resolution of the XRD analyses coupled with the presence of many mineralogical phases at elevated concentrations prevented a comprehensive identification of minerals in our samples. Hysteresis properties and temperature-dependent phase transitions ought to represent, other than magnetite, maghemite or sulphur minerals; sulphides and sulphates are naturally

incompatible minerals, but they may coexist in MSWI residues in complex phase equilibrium or perhaps disequilibrium. For example, pyrrhotite is an intermediate product of the chemical pathway to pyrite formation and arises in reductive conditions in a wide temperature window (ca. 300-1100° C; [18]) which roughly corresponds to that encountered in different stages of a MSWI system. Sulphide minerals, especially those of the pyrite group, may end up in the municipal solid waste feed as they are essential for various applications such as, cathode material in Li-batteries, semiconductors, and photovoltaic solar panels. Besides iron oxides, care should also be given to sulphur-related pollution which is an important factor of risk associated with lung cancer and cardiopulmonary mortality [2].

In summary, the integration of information from our magnetic and non-magnetic techniques leads us to conclude that the dominant magnetic carrier in our samples is magnetite and its intermediate/impure forms (e.g., titanomagnetite, maghemite, titanohematite, and ferrite), while sulphates/sulphides (monoclinic pyrrhotite, magnetic Fe^{3+} sulphate) and carbonates are important ancillary magnetic carriers. This might strongly affect the magnetic properties of MSWI ashes and, in turn, prevent an efficient use of many fundamental magnetic plots that have to be regarded with caution.

4.2 Anthropogenic pollution and SP nanoparticles

A distinct magnetic signature characterises BA and FA generated in MSWI plants as it was predicted in a preliminary study [31]. Relatively high values of χ and κ_{FD} are characteristic parameters of MSWI ashes. Measurements of the field- and temperature-dependence of induced and remanent magnetisation show discernable differences between BA and FA samples. It has been proven that BA and FA's magnetic properties notably differ from those of loess, sediments, or soil resulting from natural processes [11] as well as other anthropogenic sources of pollution, such as coal fly ashes, dust from power stations or Fe-smelters, and landfill leachates [18]. The present study thus provides reference data for discriminating anthropogenic ferrimagnetic particles originated from MSWI systems.

The most important finding is the observed SP behaviour of BA and FA materials. The κ_{FD} parameter readily detected a contribution of SP particles and can be a reliable indicator for the preliminary assessment of the SP potential of MSWI ashes. Indeed, measurements of frequency-dependent susceptibility performed on-site can serve as a fast and cost-effective tool for monitoring SP nanoparticles. The SP fraction of BA and FA materials was confirmed and semi-quantitatively determined by temperature-dependent measures. The results presented above for SP concentrations

(Fig. 7), which provide output predictions for four national MSWI facilities, were obtained using representative samples from the first half-year of waste production. A SP amount of up to 31% (for FA) is alarming, but the dusty nature of MSWI ashes is well-known and routinely complicates their safe management. The estimated amounts of ultrafine particles are consistent with other works that revealed more than half of the FA material is submicron-sized, according to laser grain-size analysis [29]. SP-sized grains in MSWI ashes are unlikely to be detected by non-magnetic techniques; in fact, we suppose that the SP fraction, being associated with a population of large ferrimagnetic MD particles, either occurs as a coating of MD particles, as argued for traffic-related particulate matter [6], or agglomerates during re-deposition [53]. As such, SP magnetic state does not mean ultrafine particles readily available to mobilization and transport. The different analytical sensitivities to grain-size and mineralogy highlight the importance of combined approaches to assess the nano-pollution related to SP grains in MSWI ashes. The following estimates assume the SP fraction is made of discrete grains and are intended to raise awareness about potential risks and to further our understanding on this particular kind of anthropogenic material. Taking the average of MSWI BA and FA outputs ($3.5 \cdot 10^4$ t/a and $4.1 \cdot 10^3$ t/a, respectively [33]) and the estimated SP concentrations according to Banerjee's graphical method on low-temperature demagnetization curves, we obtain a SP fraction ranging 5.6-7.7 (BA) and 1.0-1.3 (FA) kilo tons/year. These figures are indicative of the SP annual flow from solid ashes of a typical MSWI system and translate to ~$45 \cdot 10^4$ tons/year SP grains (as a maximum range value) discharged every year by a medium-sized country running 50 MSWI plants. The overall SP contribution is likely underestimated and does not include the SP fraction that is not retained by the MSWI filters and escapes in the atmosphere. Buonanno et al. concluded that the ultrafine particle emission from waste incinerators is negligible and that the efficiency of the filtration devices is relatively high [30]. However, their review relies on a limited number of studies based on non-magnetic methods. Considering an average of $1.03 \cdot 10^5$ t/a of particulate vapour escaping from the smokestack of a typical MSWI plant [33] and a conservative 10% SP estimate included in this particulate emission, a resulting SP fraction in the order of 10^4 t/a is realistic and significant in a long-term view. We can surmise that agglomeration and clamping of smaller SP grains with larger ones favour the filtration efficiency and decrease the inhalation risk. Nonetheless, the SP fraction estimates stress the risk related to re-suspended dust during handling and recycling processes. It was not in the scope of this study to assess the SP particulate emissions via air-quality monitoring systems or whether our estimates on solid outputs are directly related to the size of the MSWI facilities, system designs, or waste feed compositions, but certainly, that would be the objective of future research.

Given these premises, it is logical that the numerous MSWI facilities producing huge amounts of solid residues and particulate vapour have a significant impact on urban areas. The inhalation risk related to nanoparticles from MSWI hot spots may have a severe effect locally (within 50 km distance) although sulphur species could overcome larger distances [23]. As such, ultrafine pollution from waste incineration may add to the general particulate pollution from a range of outdoor sources (e.g., traffic) to which people are exposed. So, there is a need to calibrate the current technologies towards the safer management of incineration waste and plan new monitoring strategies that consider the use of magnetic methods. Alterations to the combustion process or the implementation of secondary treatment technologies may render the MSWI systems more environmentally secure and the MSWI ashes better suited for handling, reuse, or long-term landfilling.

ACKNOWLEDGMENTS

The authors gratefully acknowledge the following people for their valuable assistance during measurements/interpretation: Mike Jackson, Dario Bilardello, Peter Solheid, and Bruce Moskowitz (Institute for Rock Magnetism – IRM, Minneapolis), Giorgio Gasparotto and Giovanni Valdré (BiGeA Department – Bologna). We sincerely thank Mike Jackson (Institute for Rock Magnetism – IRM, Minneapolis) for reviewing the first draft of this manuscript. Special thanks are due to the Associate Editor Kevin V. Thomas for handling the manuscript, and to Aldo Winkler and three anonymous referees for their helpful comments.

An IRM Visiting Fellowship granted to V.F. allowed performing part of this work at the Institute for Rock Magnetism (IRM) at the University of Minnesota. The IRM is a US National Multi-user Facility supported through the Instrumentation and Facilities program of the National Science Foundation, Earth Sciences Division, and by funding from the University of Minnesota.

REFERENCES

1. W.H.O., *World Health Organization. Health effects of particulate matter. Policy implications for countries in eastern Europe, Caucasus and central Asia*. http://www.euro.who.int/en/health-topics/environment-and-health/air-quality/publications/2013/health-effects-of-particulate-matter.-policy-implications-for-countries-in-eastern-europe,-caucasus-and-central-asia-20132013.
2. Pope III, C.A., Burnett, R.T., Thun, M.J., Calle, E.E., Krewski, D., Ito, K., and Thurston, G.D., *Lung Cancer, Cardiopulmonary Mortality, and Long-term Exposure to Fine Particulate Air Pollution.* JAMA, 2002. **287**(9): p. 1132-1141; DOI: 10.1001/jama.287.9.1132.
3. Maher, B.A., Ahmed, I.A., Karloukovski, V., MacLaren, D.A., Foulds, P.G., Allsop, D., . . . Calderon-Garciduenas, L., *Magnetite pollution nanoparticles in the human brain.* Proceedings of the National

Academy of Sciences of the United States of America, 2016. 10.1073/pnas.1605941113; DOI: 10.1073/pnas.1605941113.
4. Thompson, R. and Oldfield, F., *Environmental Magnetism*. 1 ed. 10.1007/978-94-011-8036-81986, London: Springer Netherlands. 228.
5. Muxworthy, A.R., Schmidbauer, E., and Petersen, N., *Magnetic properties and Mössbauer spectra of urban atmospheric particulate matter: a case study from Munich, Germany.* Geophysical Journal International, 2002. **150**(2): p. 558-570.
6. Sagnotti, L. and Winkler, A., *On the magnetic characterization and quantification of the superparamagnetic fraction of traffic-related urban airborne PM in Rome, Italy*. Atmospheric Environment, 2012. **59**: p. 131-140; DOI: 10.1016/j.atmosenv.2012.04.058.
7. Zhu, Z., Li, Z., Bi, X., Han, Z., and Yu, G., *Response of magnetic properties to heavy metal pollution in dust from three industrial cities in China.* Journal of Hazardous Materials, 2013. **246-247**: p. 189-98; DOI: 10.1016/j.jhazmat.2012.12.024.
8. Hansard, R., Maher, B.A., and Kinnersley, R.P., *Rapid magnetic biomonitoring and differentiation of atmospheric particulate pollutants at the roadside and around two major industrial sites in the U.K.* Environmental Science & Technology, 2012. **46**(8): p. 4403-10; DOI: 10.1021/es203275r.
9. Dearing, J.A., Bird, P.M., Dann, R.J.L., and Benjamin, S.F., *Secondary ferrimagnetic minerals in Welsh soils: a comparison of mineral magnetic detection methods and implications for mineral formation.* Geophysical Journal International, 1997. **130**(3): p. 727-736; DOI: 10.1111/j.1365-246X.1997.tb01867.x.
10. Jordanova, N., Jordanova, D., Veneva, L., Yorova, K., and Petrovsky, E., *Magnetic Response of Soils and Vegetation to Heavy Metal Pollutions - A Case Study*. Environmental Science & Technology, 2003. **37**: p. 4417-4424; DOI: 10.1021/es0200645.
11. Fialová, H., Maier, G., Petrovský, E., Kapička, A., Boyko, T., and Scholger, R., *Magnetic properties of soils from sites with different geological and environmental settings.* Journal of Applied Geophysics, 2006. **59**(4): p. 273-283; DOI: 10.1016/j.jappgeo.2005.10.006.
12. Wang, X., Løvlie, R., Zhao, X., Yang, Z., Jiang, F., and Wang, S., *Quantifying ultrafine pedogenic magnetic particles in Chinese loess by monitoring viscous decay of superparamagnetism.* Geochemistry, Geophysics, Geosystems, 2010. **11**(10): p. n/a-n/a; DOI: 10.1029/2010gc003194.
13. Vigliotti, L., Capotondi, L., and Torii, M., *Magnetic properties of sediments deposited in suboxic-anoxic environments: relationships with biological and geochemical proxies.* Geological Society, London, Special Publications, 1999. **151**(1): p. 71-83; DOI: 10.1144/gsl.sp.1999.151.01.08.
14. Zhang, C., Qiao, Q., Piper, J.D., and Huang, B., *Assessment of heavy metal pollution from a Fe-smelting plant in urban river sediments using environmental magnetic and geochemical methods.* Environmental Pollution, 2011. **159**(10): p. 3057-70; DOI: 10.1016/j.envpol.2011.04.006.
15. Veneva, L., Hoffmann, V., Jordanova, D., Jordanova, N., and Fehr, T., *Rock magnetic, mineralogical and microstructural characterization of fly ashes from Bulgarian power plants and the nearby anthropogenic soils.* Physics and Chemistry of the Earth, Parts A/B/C, 2004. **29**(13-14): p. 1011-1023; DOI: 10.1016/j.pce.2004.03.011.
16. Jordanova, D., Jordanova, N., and Hoffmann, V., *Magnetic mineralogy and grain-size dependence of hysteresis parameters of single spherules from industrial waste products.* Physics of the Earth and Planetary Interiors, 2006. **154**(3-4): p. 255-265; DOI: 10.1016/j.pepi.2005.06.015.
17. Lu, S.G., Chen, Y.Y., Shan, H.D., and Bai, S.Q., *Mineralogy and heavy metal leachability of magnetic fractions separated from some Chinese coal fly ashes.* Journal of Hazardous Materials, 2009. **169**(1-3): p. 246-55; DOI: 10.1016/j.jhazmat.2009.03.078.
18. Magiera, T., Jabłońska, M., Strzyszcz, Z., and Rachwal, M., *Morphological and mineralogical forms of technogenic magnetic particles in industrial dusts.* Atmospheric Environment, 2011. **45**(25): p. 4281-4290; DOI: 10.1016/j.atmosenv.2011.04.076.
19. Moskowitz, B.M., Jackson, M., and Chandler, V., *Geophysical Properties of the Near-Surface Earth: Magnetic Properties.* 2015. In: Treatise on Geophysics, Second Edition: p. 139-174; DOI: 10.1016/b978-0-444-53802-4.00191-3.
20. Englert, N., *Fine particles and human health--a review of epidemiological studies.* Toxicology Letters, 2004. **149**(1-3): p. 235-42; DOI: 10.1016/j.toxlet.2003.12.035.

21. Solaimani, P., Saffari, A., Sioutas, C., Bondy, S.C., and Campbell, A., *Exposure to ambient ultrafine particulate matter alters the expression of genes in primary human neurons.* Neurotoxicology, 2016. **58**: p. 50-57; DOI: 10.1016/j.neuro.2016.11.001.
22. Levy, J.I., Wilson, A.M., Evans, J.S., and Spengler, J.D., *Estimation of Primary and Secondary Particulate Matter Intake Fractions for Power Plants in Georgia.* Environmental Science & Technology, 2003. **37**(24): p. 5528-5536.
23. Lamancusa, C., Parvez, F., and Wagstrom, K., *Spatially resolved intake fraction estimates for primary and secondary particulate matter in the United States.* Atmospheric Environment, 2017. **150**: p. 229-237; DOI: 10.1016/j.atmosenv.2016.11.010.
24. Szuszkiewicz, M., Magiera, T., Kapička, A., Petrovský, E., Grison, H., and Gołuchowska, B., *Magnetic characteristics of industrial dust from different sources of emission: A case study of Poland.* Journal of Applied Geophysics, 2015. **116**: p. 84-92; DOI: 10.1016/j.jappgeo.2015.02.027.
25. Huliselan, E.K., Bijaksana, S., Srigutomo, W., and Kardena, E., *Scanning electron microscopy and magnetic characterization of iron oxides in solid waste landfill leachate.* Journal of Hazardous Materials, 2010. **179**(1-3): p. 701-8; DOI: 10.1016/j.jhazmat.2010.03.058.
26. Cernuschi, S., Giugliano, M., Ozgen, S., and Consonni, S., *Number concentration and chemical composition of ultrafine and nanoparticles from WTE (waste to energy) plants.* Science of the Total Environment, 2012. **420**: p. 319-26; DOI: 10.1016/j.scitotenv.2012.01.024.
27. Funari, V., Bokhari, S.N., Vigliotti, L., Meisel, T., and Braga, R., *The rare earth elements in municipal solid waste incinerators ash and promising tools for their prospecting.* Journal of Hazardous Materials, 2016. **301**: p. 471-479; DOI: 10.1016/j.jhazmat.2015.09.015.
28. C.P.P., *Committee for Prevention and Precaution. Municipal Solid Waste Incinerators: Risks and Policies*, M.o.E.a.S. Development, Editor. 2004, Ministry of Ecology and Sustainable Development: Paris, France. p. 1-57.
29. De Boom, A. and Degrez, M., *Belgian MSWI fly ashes and APC residues: a characterisation study.* Waste Management, 2012. **32**(6): p. 1163-70; DOI: 10.1016/j.wasman.2011.12.017.
30. Buonanno, G. and Morawska, L., *Ultrafine particle emission of waste incinerators and comparison to the exposure of urban citizens.* Waste Management, 2015. **37**: p. 75-81; DOI: 10.1016/j.wasman.2014.03.008.
31. Funari, V., *Magnetic characterization of solid by-products from Municipal Solid Waste Incinerators.* The IRM Quarterly, 2016. **26**(2): p. 2-3, http://www.irm.umn.edu/quarterly/irmq26-2.pdf.
32. Funari, V., Braga, R., Bokhari, S.N., Dinelli, E., and Meisel, T., *Solid residues from Italian municipal solid waste incinerators: A source for "critical" raw materials.* Waste Management, 2015. **45**: p. 206-216; DOI: 10.1016/j.wasman.2014.11.005.
33. Funari, V., Meisel, T., and Braga, R., *The potential impact of municipal solid waste incinerators ashes on the anthropogenic osmium budget.* Science of the Total Environment, 2016. **541**: p. 1549-1555; DOI: 10.1016/j.scitotenv.2015.10.014.
34. Eusden, J.D., Eighmy, T.T., Hockert, K., Holland, E., and Marsella, K., *Petrogenesis of municipal solid waste combustion bottom ash.* Applied Geochemistry, 1999. **14**(8): p. 1073-1091; DOI: 10.1016/S0883-2927(99)00005-0.
35. Bayuseno, A.P. and Schmahl, W.W., *Understanding the chemical and mineralogical properties of the inorganic portion of MSWI bottom ash.* Waste Management, 2010. **30**(8–9): p. 1509-1520; DOI: http://dx.doi.org/10.1016/j.wasman.2010.03.010.
36. Bogush, A., Stegemann, J.A., Wood, I., and Roy, A., *Element composition and mineralogical characterisation of air pollution control residue from UK energy-from-waste facilities.* Waste Management, 2015. **36**: p. 119-29; DOI: 10.1016/j.wasman.2014.11.017.
37. Greenwood, N.N. and Gibb, T.C., *Mössbauer Spectroscopy*. 10.1007/978-94-009-5697-11971, London: Springer Netherlands.
38. Zyryanov, V.V., Petrov, S.A., and Matvienko, A.A., *Characterization of spinel and magnetospheres of coal fly ashes collected in power plants in the former USSR.* Fuel, 2011. **90**(2): p. 486-492; DOI: 10.1016/j.fuel.2010.10.006.

673 39. Gomes, S., François, M., Abdelmoula, M., Refait, P., Pellissier, C., and Evrard, O., *Characterization of magnetite in silico-aluminous fly ash by SEM, TEM, XRD, magnetic susceptibility, and Mössbauer spectroscopy.* Cement and Concrete Research, 1999. **29**(11): p. 1705-1711.
676 40. Fermo, P., Cariati, F., Pozzi, A., Demartin, F., Tettamanti, M., Collina, E., . . . Russo, U., *The analytical characterization of municipal solid waste incinerator fly ash: methods and preliminary results.* Fresenius Journal of Analytical Chemistry, 1999: p. 365 : 666–673.
679 41. Roberts, A.P., Pike, C.R., and Verosub, K.L., *First-order reversal curve diagrams: A new tool for characterizing the magnetic properties of natural samples.* Journal of Geophysical Research: Solid Earth, 2000. **105**(B12): p. 28461-28475; DOI: 10.1029/2000jb900326.
682 42. Muxworthy, A.R., *Assessing the ability of first-order reversal curve (FORC) diagrams to unravel complex magnetic signals.* Journal of Geophysical Research, 2005. **110**(B1); DOI: 10.1029/2004jb003195.
685 43. Roberts, A.P., Liu, Q., Rowan, C.J., Chang, L., Carvallo, C., Torrent, J., and Horng, C.-S., *Characterization of hematite (α-Fe2O3), goethite (α-FeOOH), greigite (Fe3S4), and pyrrhotite (Fe7S8) using first-order reversal curve diagrams.* Journal of Geophysical Research: Solid Earth, 2006. **111**(B12): p. 1-16; DOI: 10.1029/2006jb004715.
689 44. Harrison, R.J. and Feinberg, J.M., *FORCinel: An improved algorithm for calculating first-order reversal curve distributions using locally weighted regression smoothing.* Geochemistry, Geophysics, Geosystems, 2008. **9**(5): p. 1-11; DOI: 10.1029/2008gc001987.
692 45. Magiera, T. and Strzyszcz, Z., *Ferrimagneticminerals of anthropogenic origin in Soils of some polish national parks.* Water Air and Soil Pollution, 2000. **124**: p. 37-48.
694 46. Maher, B.A. and Taylor, R.M., *Formation of ultrafine-grained magnetite in soils.* Letters to nature, 1988. **336**: p. 368 - 370; DOI: 10.1038/336368a0.
696 47. Banerjee, S.K., Hunt, C.P., and Liu, X.-M., *Separation of local signals from the regional paleomonsoon record of the chinese loess plateau: a rock-magnetic approach.* Geophysical Research Letters, 1993. **20**(9): p. 843-846.
699 48. Hunt, C.P., Banerjee, S.K., Han, J., Solheid, P.A., Oches, E., Sun, W., and Liu, T., *Rock-magnetic proxies of climate change in the loess-palaeosol sequences of the western Loess Plateau of China.* Geophysical Journal International, 1995. **123**: p. 232-244.
702 49. Bilardello, D. and Jackson, M., *What do the Mumpsies do?* The IRM Quarterly, 2013. **23**(3): p. 1-16, http://www.irm.umn.edu/quarterly/irmq23-3.pdf.
704 50. Jackson, M., Sagnotti, L., Rochette, P., and Sølheid, P., *Maintaining Standards III: Pozzolana Cement cross-calibration samples available.* The IRM Quarterly, 2003. **13**(3): p. 1-12.
706 51. Özdemir, Ö., Dunlop, D.J., and Berquó, T.S., *Morin transition in hematite: Size dependence and thermal hysteresis.* Geochemistry, Geophysics, Geosystems, 2008. **9**(10): p. 1-12; DOI: 10.1029/2008gc002110.
709 52. Smirnov, A.V. and Tarduno, J.A., *Estimating superparamagnetism in marine sediments with the time dependency of coercivity of remanence.* Journal of Geophysical Research: Solid Earth, 2001. **106**(B8): p. 16135-16143; DOI: 10.1029/2001jb000152.
712 53. He, X., Mitrano, D.M., Nowack, B., Bahk, Y.K., Figi, R., Schreiner, C., . . . Wang, J., *Agglomeration potential of TiO2 in synthetic leachates made from the fly ash of different incinerated wastes.* Environmental Pollution, 2017. **223**: p. 616-623; DOI: 10.1016/j.envpol.2017.01.065.

715

716